

Interaction of Metals with Well-Defined Oxides: Understanding the Role of Surface Defects on Metal Interactions and Measuring Metal Nanoparticle Energetics

Introduction:

Metal films and particles on oxide surfaces are important in many industrial applications, such as heterogeneous catalysis^[1], microelectronics^[2], and photovoltaic devices^[3]. Active industrial processes apply catalysts consisting of metal nanoparticles supported on oxides to a variety of important reactions.^[4-8] The reaction typically takes place on the metal particles, but their interaction with the underlying support is thought to be critical for some systems. In many cases the oxide-supported nanoparticle catalysts are rendered inoperable due to particle sintering. One key to improving these types of catalysts is therefore to fundamentally understand the interaction between the supported nanoparticles and the oxide surface.

The goal of our research is to measure the strength of the interaction between metal nanoparticles and the oxide support. One method to measure this strength is temperature programmed desorption (TPD). However, on oxide surfaces transition metals sinter before the metal desorbs in TPD, providing no information about the strength of the metal-to-oxide interface on the un-sintered (smaller) metal particles.^[9, 10] Measuring this interaction is possible using calorimetric techniques in ultrahigh vacuum (UHV). Early UHV calorimetry techniques used polycrystalline samples, whose surfaces were not well-defined.^[11] King's group created the first single-crystal UHV adsorption calorimeter, which measured the emitted infrared radiation due to heating by adsorbed molecules on a thin single-crystal.^[12] The Campbell group improved on King's design, enabling high temperature annealing (for cleaning purposes), and enabling low temperature calorimetry measurements (for adsorbates that have low sticking probabilities on room temperature single-crystals).^[9] The calorimeter we use for this research is unique in its ability to directly measure the heat released when metal atoms adsorb onto well-defined oxide surfaces.

We apply calorimetry to answer fundamental questions on the interaction between metal nanoparticles and the oxide surface support: what is the heat of adsorption of a metal onto an oxide surface, how does this depend on the size of the metal cluster to which it attaches and the nature of the oxide surface, and how the energetics, reactivity, and electronic properties vary with metal coverage?^[1] In addition, by varying the deposited metal we can show if any periodic trends for metal-to-oxide energetics can be observed. Answering these questions could lead to the development of sinter resistant catalysts, and improvements in catalysis designs.

Previous studies in our group measured metal atom adsorption onto MgO(100). Three metals have been deposited onto this oxide film: Cu, Pb, and Ag.^[10] These studies found that the interaction between metal and oxide was weaker than metal-to-metal bonding: Cu on MgO(100) releases 240 kJ/mol, Pb releases 103 kJ/mol, and Ag releases 176 kJ/mol while the heat of sublimations of the metals are 337 kJ/mol, 195 kJ/mol, and 285 kJ/mol respectively [Fig. 1]. The metals were found to grow as 3D particles on MgO(100). In addition, it was noted that the sticking probability was proportional to the strength of the interaction. For example, Pb had the lowest heat of adsorption, and the lowest sticking probability. Recent density functional calculations agree with the growth model and adsorption energetics for Cu^[13] and Ag.^[14, 15] The

measurements showed that these metals would sinter rapidly on MgO(100) and would not wet the surface.

Recently we have studied the adsorption of Ca and Li onto MgO(100). These electropositive adsorbates show different adsorption behavior than the noble metals studied previously. The main difference is that these adsorbates (Ca and Li) can act as probes for the defects present on the MgO(100) surface. This allows us to measure calorimetrically the interaction between the adsorbates and the surface defects. It was observed that Ca adsorbates on MgO(100) are highly mobile, and that adsorption occurs mainly at defect sites (steps or kinks). On the other hand, Li adsorbates are less mobile due to strong Li interactions with more sites on the MgO(100) surface; including, structural defect sites (steps or kinks), oxygen vacancies, and MgO divacancies. Our experimental observations have been augmented by comparison to calculations from our collaborators at the University of Texas at Austin (Prof. Graeme Henkelman and Dr. Lijun Xu).^[16, 17]

We have also studied single-crystal oxides of CeO₂(111) grown on Pt(111). Oxides of cerium are very interesting catalytically due to the relative ease in which the oxide can be reduced.^[18-20] The reduction of ceria generates oxygen that can then be used in the catalytic processes taking place on the supported metal nanoparticles. Catalysts that leverage this ability of cerium oxides have been in use for decades (the three way auto catalytic converter used in automobiles). A new application for these reactive oxide supports is for use in fuel cell applications.^[21-25] We have measured the adsorption energetics of Ag on CeO₂(111). The measurements show that Ag interacts weakly with oxygen vacancies on CeO₂(111).

Future Plans:

We will continue to explore the interactions of metals with CeO₂(111). Experiments using a scanning tunneling microscope will be performed to observe the binding site of Ag and Cu on CeO₂(111), which will allow us to extract more information from the heat of adsorption measurements. Further heat of adsorption measurements of Ag on ceria at low temperatures (190 K) will allow us to extract the adhesion energy (important for understanding the oxide to metal bonding), and adsorption of Ag onto damaged ceria will allow us to probe defect to metal interactions. We will continue by studying the binding of catalytically interesting Cu on CeO₂(111), and through the adsorption of Ca we will continue investigating the defects on the ceria surface.

Experimental Details:

To study the oxide surface we need to ensure that the surface is clean and free from contaminants, to this end the calorimeter was installed in an UHV chamber that has been described in detail in the literature.^[26] UHV conditions (pressure <10⁻⁹ mbar) keep the surface clean during the time it takes to perform an experiment, and ensures we are studying only the interaction between metal atoms and the oxide surface. The UHV chamber is equipped with surface analysis techniques: Auger electron spectroscopy (AES), ion scattering spectroscopy (ISS), low energy electron diffraction (LEED), mass spectroscopy (MS), and a quartz crystal microbalance (QCM). Sample cleanliness was verified using AES and ISS, and its crystallinity was checked using LEED. MS was used to analyze the residual gases in the vacuum chamber and for measuring sticking probability. The QCM was used to measure the flux from the metal atom beam.

The calorimeter consists of a pyroelectric polymer (β -polyvinylidene fluoride, PVDF) ribbon that is put into contact with the back of a single-crystal [Fig. 2]. The heat released by the adsorption of gas phase species generates a voltage pulse on the ribbon. The voltage pulse is then amplified and recorded on a computer. A He-Ne laser of known power is used to calibrate the voltage pulse from the adsorbing atoms.

Gas phase atoms are generated in an effusive vapor source from high purity metals. The vapor is collimated through a series of three water-cooled apertures in order to generate a deposition spot of ~ 4 mm in diameter on the single-crystal [Fig. 3]. The collimated beam is chopped into 0.1 second pulses which delivers ~ 0.01 of a ML (a ML is $\sim 1 \times 10^{15}$ atoms/cm²) every 2 seconds [Fig. 4]. The flux from the effusive source is measured using a QCM that can be positioned between the source and the single-crystal. It is also necessary to measure the portion of the incident flux that does not stick to the single-crystal; this sticking probability is measured by MS during deposition.

The metal atom beam strikes a single-crystal oxide thin-film that is grown onto a Mo(100) single-crystal. The Mo(100) crystal is one micron thick and 10 mm in diameter. The crystal was cleaned using a combination of Ar⁺ bombardment and high temperature annealing (>1400 °C) prior an experiment. The MgO(100) thin-films are grown using the recipe of Wu et al.; in short, Mg vapor is generated from a resistively heated Ta boat containing a rod of Mg, which is deposited in a background pressure of oxygen.^[27] The films are grown to ~ 4 nm in thickness (as measured using AES). A new MgO(100) thin-film is grown for each experiment in order to avoid contamination from previous experiments.

References:

1. Campbell, C. T., *Faraday Transactions*, **1996**. 92, 9, 1435-1445.
2. Yang, J. Y., Kim, J.H.; Choi, W.J.; Do, Y.H.; Kim, C.O.; Hong, J.P., *Journal of Applied Physics*, **2006**. 100, 066102.
3. He, T., Ma, Y.; Cao, Y.; Yin, Y.; Yang, W.; Yao, J., *Applied Surface Science*, **2001**. 180, 3-4, 336-340.
4. Iglesia, E., *Applied Catalysis A*, **1997**. 161, 59-78.
5. Shen, W. J., Ichihashi, Y.; Matsumura, Y., *Catalysis Letters*, **2002**. 79, 125-127.
6. Matsumura, Y. S., Ichihashi, Y., Okumura, M., *J. Catal.*, **2001**. 197, 267-272.
7. de Oliveira, A. L., Wolf, A.; Schuth, F., *Catalysis Letters*, **2001**. 73, 157-160.
8. Rodriguez, J. A., Liu, G.; Jirsak, T.; Hrbek, J.; Chang, Z. P.; Dvorak, J.; Maiti, A., *J. Am. Chem. Soc.*, **2002**. 124, 5242-5250.
9. Stuckless, J. T., Starr, D. E.; Campbell, C. T., *J. Chem. Phys.*, **1997**. 107, 14, 5547-5553.
10. Campbell, C. T., Starr, D. E., *J. Am. Chem. Soc.*, **2002**. 124, 9212-9218.
11. Eley, D. D., Norton, P.R., *Proc. Royal Soc. London Series A*, **1970**. 314, 1518, 301-318.
12. Borroni-Bird, C. E., King, D.A., *Review of Scientific Instruments*, **1991**. 62, 9, 2177-2185.
13. Zhukovskii, Y. F., Kotomin, E.A.; Fuks, D.; Dorfman, S.; Stoneham, A.M.; Sychev, O.; Borstel, G., *Applied Surface Science*, **2004**. 226, 298-305.
14. Zhukovskii, Y. F., Kotomin, E.A.; Fuks, D.; Dorfman, S., *Superlattices and Microstructures*, **2004**. 36, 1-3, 63-72.
15. Giordano, L., Baistrocchi, M.; Pacchioni, G., *Phys. Rev. B*, **2005**. 72, 115403.
16. Zhu, J. F., Farmer, J.A.; Ruzycski, N.; Campbell, C.T., *J. Am. Chem. Soc.*, **2008**, In preparation.
17. Farmer, J. A., Ruzycski, N.; Campbell, C.T., **2008**, In preparation.
18. Xiao, W., Guo, Q.; Wang, E.G., *Chem. Phys. Lett.*, **2003**. 368, 527-531.
19. Pfau, A., Schierbaum, K.D., *Surface Science*, **1994**. 321, 71-80.
20. Berner, U., Schierbaum, K.D.; Jones, G.; Wincott, P.; Haq, S.; Thornton, G., *Surface Science*, **2000**. 467, 201-213.
21. Avgouropoulos, G., Papavasiliou, J.; Tabakova, T.; Idakiev, V.; Ioannides, T., *Chem. Engr. J.*, **2006**. 124, 41-45.
22. Zheng, X., Zhang, X.; Fang, Z.; Wang, X.; Wang, S.; Wu, S., *Catalysis Communications*, **2006**. 7, 701-704.
23. Yang, Y., Xu, X.; Sun, S., *Catalysis Communications*, **2006**. 7, 756-760.
24. Wang, J. H., Liu, M.; Lin, M.C., *Solid State Ionics*, **2006**. 177, 939-947.
25. Itome, M., Nelson, A.E., *Catalysis Letters*, **2006**. 106, 1-2, 21-27.
26. Stuckless, J. T., Frei, N.A.; Campbell, C. T., *Review of Scientific Instruments*, **1998**. 69, 6, 2427-2438.
27. Wu, M. C., Corneille, J.S.; He, J.W.; Estrada, C.A.; Goodman, D.W., *JVSTA*, **1992**. 10, 4, 1467-1471.

Figures:

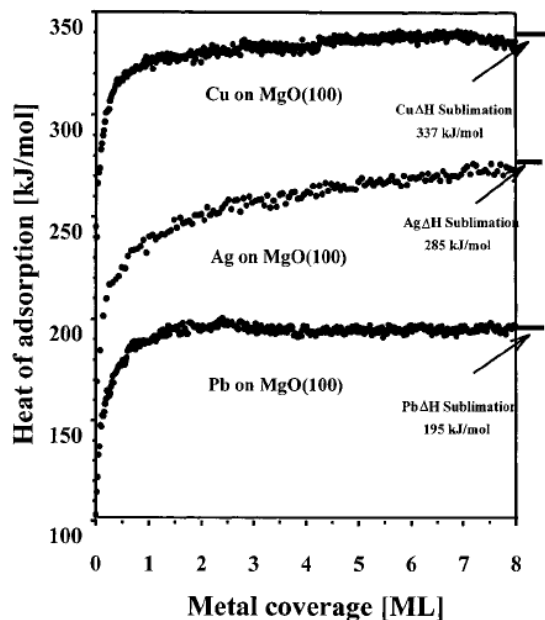


Figure 1: Heat of adsorption of Cu, Ag, and Pb onto MgO(100) at 300 K.^[10]

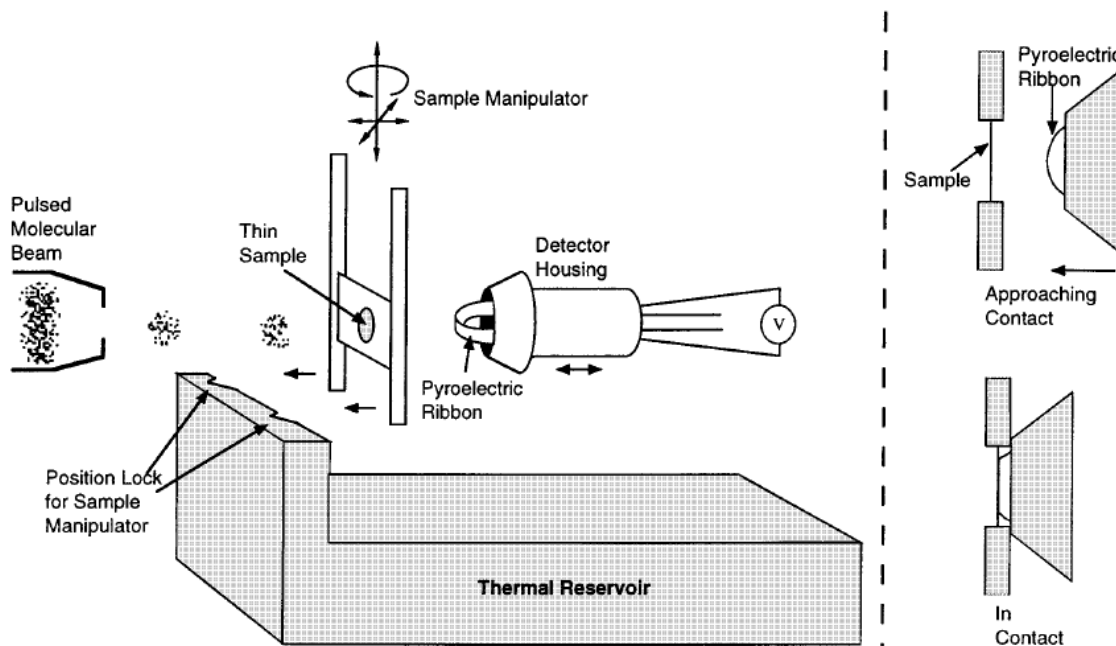


Figure 2: Schematic showing UHV calorimeter, single-crystal sample holder, and metal atom beam. The two figures on the right show how contact is made between the single-crystal and the pyroelectric ribbon.^[26]

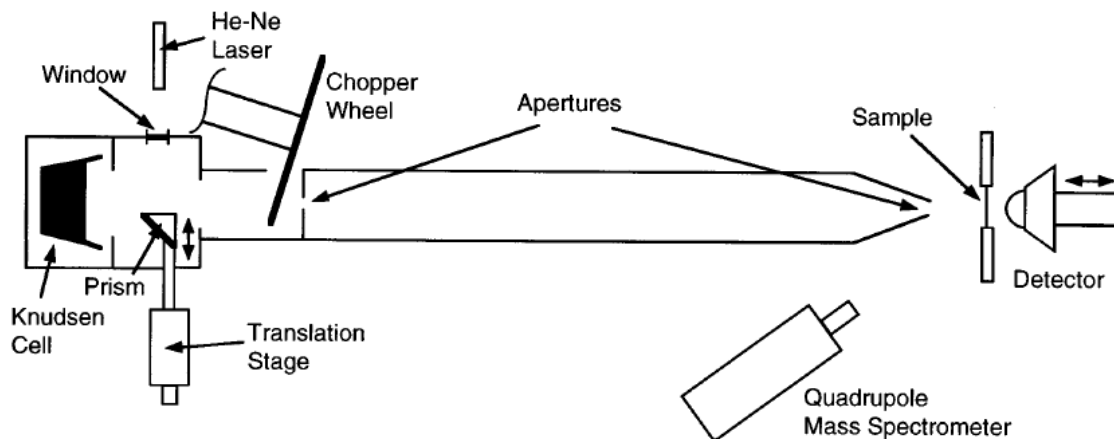


Figure 3: Schematic of the metal atom beam source. Showing the effusion source (Knudsen cell), prism and He-Ne laser for heat detector calibrations, and the chopper wheel and apertures which generate the pulsed collimated beam.^[26]

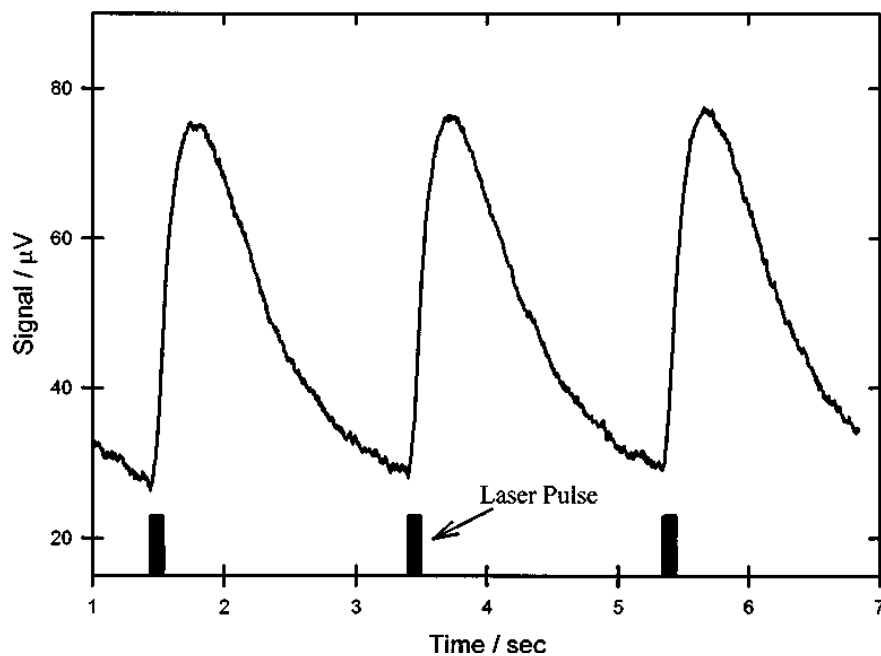


Figure 4: Pyroelectric ribbon response to a train of three laser pulses. The black bars represent the time span that the sample was exposed to the laser source (100 ms). The trace corresponds to the voltage response of the ribbon to the heat input.¹⁶